IECON2015-Yokohama
November 9-12, 2015

Eigenvalue-based Harmonic Stability Analysis Method in Inverter-Fed Power Systems

Yanbo Wang, Xiongfei Wang, Frede Blaabjerg, Zhe Chen
Department of Energy Technology
Aalborg University
Aalborg, Denmark
ywa@et.aau.dk, xwa@et.aau.dk, fbl@et.aau.dk, zch@et.aau.dk

Abstract — **This paper presents an eigenvalue-based harmonic stability analysis method for inverter-fed power systems. A full-order small-signal model for a droop-controlled Distributed Generation (DG) inverter is built first, including the time delay of digital control system, inner current and voltage control loops, and outer droop-based power control loop. Based on the inverter model, an overall small-signal model of a two-inverter-fed system is then established, and the eigenvalue-based stability analysis is subsequently performed to assess the influence of controller parameters on the harmonic resonance and instability in the power system. Eigenvalues associated with time delay of inverter and inner controller parameters is obtained, which shows the time delay has an important effect on harmonic instability of inverter-fed power systems. Simulation results are given for validating the proposed harmonic stability analysis method.**

Keywords—Harmonic Stability; Eigenvalue; Time Delay; Small Signal model; Inverter-Interfaced Power System

I. INTRODUCTION

The proportion of renewable energy in power systems has been increasing in recent years [1]. Inverter-fed power systems are playing a significant role in modern electric grid [2]. Various forms of distributed generators such as wind farm [3], PV plant [4], and microgrids [5] are interfaced to power grid by power converters. These small scale power systems can provide reliability and sustainability for electricity services [6]-[7].

One of the important concerns in inverter-fed power systems is stability issue. A large number of previous stability studies focus on low-frequency oscillations resulting from droop-based power controller [7], constant power load [8] as well as phase-locked loop (PLL) [9]. In addition to low frequency stability, harmonic frequency oscillations have recently been reported in [10]-[11]. The harmonic instability phenomena result from interaction among voltage, current loops of converter, and passive components [6], where oscillations happen from hundreds of hertz to several kilohertz. This harmonic-frequency oscillation would propagate into the whole power system and worsen system power quality [6], [11].

Hence, it is necessary to develop modeling and analysis method for the harmonic stability phenomena. A common tool for assessing small signal stability is to linearize system models in operating point and form state space models. Then, stability could be investigated by means of analyzing eigenvalues in state matrix. The small signal model of a multi-bus islanded microgrid considering network voltages response were developed in [5], where the voltage control input is embedded and integrated to the small signal model. A small signal model of inverter-interfaced microgrid was built in [7], where the oscillatory modes and mode shapes based on eigenvalues and eigenvectors are identified. Small signal stability for islanded microgrids with active loads is investigated in [8], where the influence of voltage controller on system stability is studied. However, harmonic-frequency stability was not analyzed yet in aforementioned references.

To deal with harmonic stability issue, an impedance-based analytical approach was developed for an inverter-interfaced power system including multiple current- and voltage-controlled inverters with LCL- and LC-filters [6]. The impedance-based approaches were introduced in [12], which is able to assess locally system stability based on the ratio of the output impedance of the component or the equivalent system impedance [12]. However, it is difficult to reveal harmonic-frequency damping characteristic for the impedance-based approach.

The aim of this paper is to assess harmonic instability of the system. The eigenvalue analysis is performed based on small signal model of inverters considering time delay of inverter. The main contributions of this paper are: (1) Time delay of inverter is modeled by pade approximation; (2) The effect of inverter time delay and inner controller parameters on harmonic instability is analyzed.

II. SMALL SIGNAL MODELLING OF INVERTER-FED POWER SYSTEMS

This section first describes an inverter-fed power system configuration in this study. And small signal model of single DG unit is built, including current loop, voltage loop, power loop and time delay of inverter. Moreover, the overall small signal model of the system is established.

A. System Description

Fig. 1 shows the exemplified three-phase inverter-interfaced power system, where two voltage-controlled inverters are connected to network with three load buses. This work focuses on the harmonic instability caused by the dynamic interactions of inner control loops.

978-1-4799-1762-4/15/$31.00 ©2015 IEEE 003277

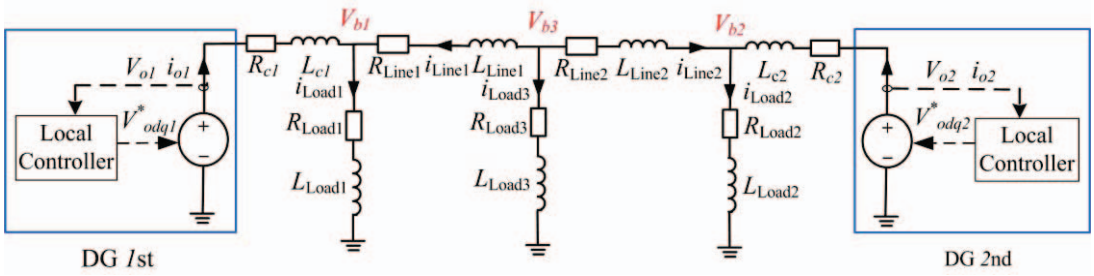

Fig. 1 The studied system configuration

B. Small Signal Modelling of DG Unit

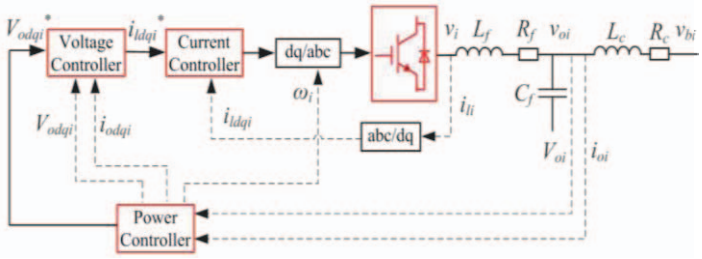

Fig. 2 DG unit block diagram with multi-loop control approach.

The previous small signal model have been intensively reported in [1],[3],[9], where inner current controller, voltage controller, power controller and loads are modeled in details. However, time delay of inverter is commonly ignored. A small signal model considering time delay of inverter will be established in this section. Fig. 2 shows the components of DG unit, which is composed of inverter time delay, voltage controller, current controller, power controller, LC filter and coupling inductance.

1) Time Delay of Inverter

Time delay of inverter is ignored assuming inverter produces ideal demanded voltage in previous work. Time delay depicts the influence of the digital computation delay and pulse width modulation (PWM) delay [13]. In fact, time delay of inverter maybe has an important influence on harmonic-frequency stability [5], which can be modelled as (1)

$$v_i = e^{-\tau \bullet s} v_i^* \tag{1}$$

,where v_i^* and v_i are demanded voltage and inverter output voltage, respectively. $\tau = 1.5T_s$ is delay time resulting from digital computation delay (T_s) and the pulse width modulation (PWM) delay (0.5 T_s) [13], T_s is inverter sampling period.

To assess the influence of inverter delay, Pade approximation is employed to equivalent time delay of inverter. Pade approximation is a technique approximating delay plant, where the exponential term can be approximated as transfer function form (2).

$$e^{-\tau \bullet s} = \frac{b_0 + b_1 \tau s + \cdots + b_l (\tau s)^l}{a_0 + a_1 \tau s + \cdots + a_k (\tau s)^k} \tag{2}$$

, where $a_j = \dfrac{(l+k-j)!k!}{j!(k-j)!}$, $b_j = (-1)^j \dfrac{(l+k-j)!l!}{j!(l-j)!}$

Pade approximation (2) could be converted into state space form (3)

$$\Delta \dot{x}_{di} = A_d \Delta x_{di} \tag{3}$$

$$A_d = \begin{bmatrix} 0 & 1 & 0 & \cdots & 0 \\ 0 & 0 & 1 & \cdots & 0 \\ \vdots & \vdots & \vdots & \ddots & \vdots \\ 0 & 0 & 0 & 0 & 1 \\ \dfrac{-a_0\tau^{-k}}{a_k} & \dfrac{-a_1\tau^{-k+1}}{a_k} & \dfrac{-a_2\tau^{-k+2}}{a_k} & \cdots & \dfrac{-a_{k-1}\tau^{-1}}{a_k} \end{bmatrix}$$

l and k are the order of pade approximation. In this work, the order is chosen as $l = k = 3$. Mathematical computation for pade approximation could be implemented in MATLAB. Δx_{di} is inverter delay states. Eigenvalues of the state matrix A_d in (3) indicates harmonic-frequency dynamic associated with time delay. The influence from time delay on eigenvalue trace will be shown and discussed later.

The small signal model of time delay will be integrated to the overall small signal model.

2) Voltage Controller and Current Controller

In this work, voltage and current control loops are performed by classical PI controllers [7]. The modeling procedure of DG unit can be referred in [7]. Fig. 3 shows the block diagram of voltage controller and current controller respectively.

The state equations and output equations of voltage controller can be represented according to control diagram shown in Fig. 3(a) as (4) - (6):

$$\dot{\varphi}_d = v_{od}^* - v_{od}, \quad \dot{\varphi}_q = v_{oq}^* - v_{oq} \tag{4}$$

$$i_{ld}^* = \omega C_f v_{oq} + K_{pv}(v_{od}^* - v_{od}) + K_{iv}\varphi_d \tag{5}$$

$$i_{lq}^* = -\omega C_f v_{od} + K_{pv}(v_{oq}^* - v_{oq}) + K_{iv}\varphi_q \tag{6}$$

State space form of voltage controller can be represented by linearizing (4)-(6) as (7) and (8):

$$\Delta \dot{\varphi}_{dq} = [0][\Delta \varphi_{dq}] + B_{V1}[\Delta v_{odq}^*] + B_{V2}[\Delta i_{ldq}, \Delta v_{odq}, \Delta i_{odq}]^T \tag{7}$$

$$\Delta i_{ldq}^* = C_V[\Delta \varphi_{dq}] + D_{V1}[\Delta v_{odq}^*] + D_{V2}[\Delta i_{ldq}, \Delta v_{odq}, \Delta i_{odq}]^T \tag{8}$$

$$B_{V1} = \begin{bmatrix} 1 & 0 \\ 0 & 1 \end{bmatrix}, B_{V2} = \begin{bmatrix} 0,0,-1,0,0,0 \\ 0,0,0,-1,0,0 \end{bmatrix}, C_V = \begin{bmatrix} K_{iv} & 0 \\ 0 & K_{iv} \end{bmatrix},$$

$$D_{V1} = \begin{bmatrix} K_{pv} & 0 \\ 0 & K_{pv} \end{bmatrix}, D_{V2} = \begin{bmatrix} 0,0,-K_{pv},\omega C_f,0,0 \\ 0,0,-\omega C_f,-K_{pv},0,0 \end{bmatrix}$$

As shown in Fig. 3(b), the state equations and output equations of current controller can be represented as (9)-(11)

$$\dot{\gamma}_d = i_{ld}^* - i_{ld}, \qquad \dot{\gamma}_q = i_{lq}^* - i_{lq} \tag{9}$$

$$v_{id}^* = \omega L_f i_{lq} + K_{pc}(i_{ld}^* - i_{ld}) + K_{ic}\gamma_d \tag{10}$$

$$v_{iq}^* = -\omega L_f i_{ld} + K_{pc}(i_{lq}^* - i_{lq}) + K_{ic}\gamma_q \tag{11}$$

State space form of current controller can be represented by linearizing (9)-(11) as (12) and (13):

$$\Delta\dot{\gamma}_{dq} = [0][\Delta\gamma_{dq}] + B_{C1}[\Delta i_{ldq}^*] + B_{C2}[\Delta i_{ldq}, \Delta v_{odq}, \Delta i_{odq}]^T \tag{12}$$

$$\Delta v_{idq}^* = C_C[\Delta\gamma_{dq}] + D_{C1}[\Delta i_{ldq}^*] + D_{C2}[\Delta i_{ldq}, \Delta v_{odq}, \Delta i_{odq}]^T \tag{13}$$

$$B_{C1} = \begin{bmatrix} 1 & 0 \\ 0 & 1 \end{bmatrix},\ B_{C2} = \begin{bmatrix} -1,0,0,0,0,0 \\ 0,-1,0,0,0,0 \end{bmatrix},\ C_C = \begin{bmatrix} K_{ic} & 0 \\ 0 & K_{ic} \end{bmatrix}$$

$$D_{C1} = \begin{bmatrix} K_{pc} & 0 \\ 0 & K_{pc} \end{bmatrix},\ D_{C2} = \begin{bmatrix} -K_{pc}, \omega L_f, 0,0,0,0 \\ -\omega L_f, -K_{pc}, 0,0,0,0 \end{bmatrix}$$

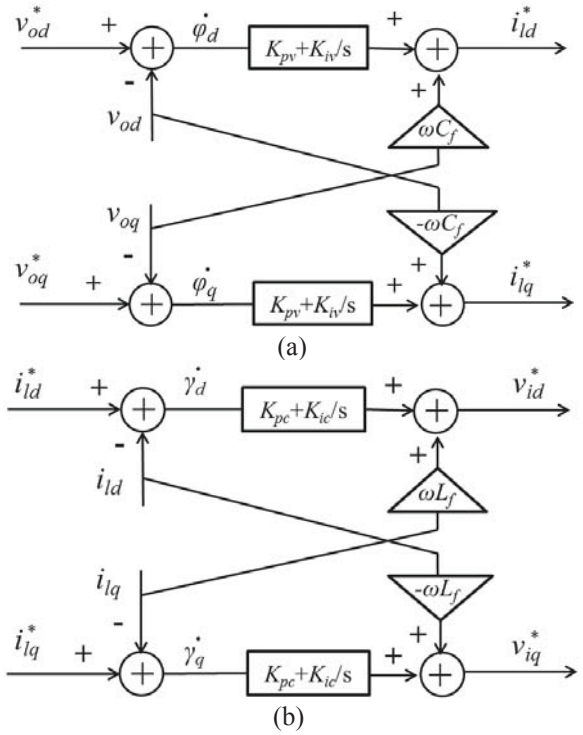

Fig. 3 The block diagram of double loop controller. (a) Voltage controller. (b) Current controller.

3) Power Controller

Power controller is responsible for perform power control among paralleled DG units. Droop control strategy is an attractive method to implement power sharing without communication devices. As shown in Fig. 4, the power controller is composed of power calculation block, filter and droop controller. The instantaneous active and reactive power can be computed by power calculation block. The average power is obtained from instantaneous power passing low pass filter. To share the active and reactive power among paralleled inverters, artificial frequency and voltage droop is introduced to perform power sharing according to droop characteristic. V_{odqi} and i_{odqi} are output voltage and current of ith DG unit on individual frame (d-q). p_i and q_i are

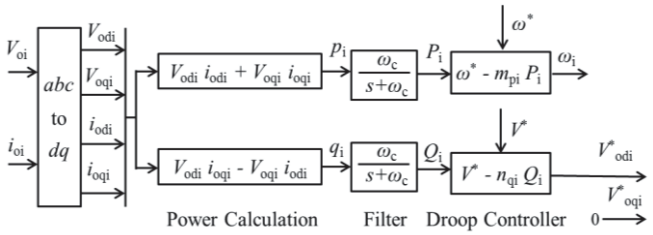

Fig. 4 The power controller of DG unit.

instantaneous active and reactive power. P_i and Q_i are average active and reactive power. ω_c is cut-off frequency of low-pass filter. m_{pi}, n_{qi} are droop coefficients of ith DG unit. Small signal modeling of the power controller could be seen in [2], [5] and [7].

(4) LC filters and coupling inductance

Small signal model of LC filter can be represented on dq frame by following state equations according to Fig. 2.

$$\frac{di_{ldi}}{dt} = -\frac{R_f}{L_f}i_{ldi} - \omega i_{lqi} + \frac{1}{L_f}v_{di} - \frac{1}{L_f}v_{odi} \tag{14}$$

$$\frac{di_{lqi}}{dt} = -\frac{R_f}{L_f}i_{lqi} + \omega i_{ldi} + \frac{1}{L_f}v_{qi} - \frac{1}{L_f}v_{oqi} \tag{15}$$

$$\frac{dv_{odi}}{dt} = -\omega v_{oqi} + \frac{1}{C_f}i_{ldi} - \frac{1}{C_f}i_{odi} \tag{16}$$

$$\frac{dv_{oqi}}{dt} = \omega v_{odi} + \frac{1}{C_f}i_{lqi} - \frac{1}{C_f}i_{oqi} \tag{17}$$

$$\frac{di_{odi}}{dt} = -\frac{R_c}{L_c}i_{odi} - \omega i_{oqi} + \frac{1}{L_c}v_{odi} - \frac{1}{L_c}v_{bdi} \tag{18}$$

$$\frac{di_{oqi}}{dt} = -\frac{R_c}{L_c}i_{oqi} + \omega i_{odi} + \frac{1}{L_c}v_{oqi} - \frac{1}{L_c}v_{bqi} \tag{19}$$

Small signal state equations of LC filter and coupling inductance could be represented by combining and linearizing (14)-(19) as (20)

$$\begin{bmatrix} \Delta\dot{i}_{ldqi} \\ \Delta v_{odqi} \\ \Delta i_{odqi} \end{bmatrix} = B_1\Delta\omega_1 + B_2\Delta v_{idq} + B_3\begin{bmatrix} \Delta i_{ldqi} \\ \Delta v_{odqi} \\ \Delta i_{odqi} \end{bmatrix} + B_4\Delta v_{bdqi} \tag{20}$$

$$B_1 = [I_{lq0}, -I_{ld0}, V_{oq0}, -V_{od0}, I_{oq}, -I_{od}]^T,\ B_2 = [-A_{12}, O_{2\times4}]^T,\ B_4 = [O_{2\times4}, -A_{31}]^T$$

$$B_3 = \begin{bmatrix} A_{11} & A_{12} & 0 \\ A_{21} & A_{22} & -A_{21} \\ 0 & A_{31} & A_{32} \end{bmatrix},\ A_{11} = \begin{bmatrix} -\frac{R_f}{L_f} & \omega_0 \\ -\omega_0 & -\frac{R_f}{L_f} \end{bmatrix},\ A_{12} = \begin{bmatrix} -\frac{1}{L_f} & 0 \\ 0 & -\frac{1}{L_f} \end{bmatrix},$$

$$A_{21} = \begin{bmatrix} \frac{1}{C_f} & 0 \\ 0 & \frac{1}{C_f} \end{bmatrix},\ A_{22} = \begin{bmatrix} 0 & \omega_0 \\ -\omega_0 & 0 \end{bmatrix},\ A_{31} = \begin{bmatrix} \frac{1}{L_c} & 0 \\ 0 & \frac{1}{L_c} \end{bmatrix},\ A_{32} = \begin{bmatrix} -\frac{R_c}{L_c} & \omega_0 \\ -\omega_0 & -\frac{R_c}{L_c} \end{bmatrix}$$

Then, a complete small signal model of an individual inverter are founded by combining small signal models of the current controller, voltage controller, power controller, inverter delay, LC filter and coupling inductance as (21).

$$\Delta\dot{x}_{invi} = A_1\Delta x_{invi} + B_1\Delta v_{bDQi} + B_{com}\Delta\omega_{com} \tag{21}$$

$$\Delta x_{invi} = \left[\Delta\delta_i, \Delta P_i, \Delta Q_i, \Delta\varphi_{dqi}, \Delta\gamma_{dqi}, \Delta i_{ldqi}, \Delta x_{di}, \Delta v_{odqi}, \Delta i_{odqi}\right](i = 1,2)$$

C. Small Signal Modeling of Overall System

To formulate small signal model of overall system shown in Fig. 1, the linearized equations of line currents and load currents should be built on the common reference frame (D-Q), which can be referred in [5] and [7].

Finally, the overall small signal model combining DG units, network, loads can be obtained as (22)

$$\Delta \dot{x} = A\Delta x \tag{22}$$

Δx is the overall microgrid state vector. A is system state matrix. $\Delta x = \left[\Delta x_{inv1}, \Delta x_{inv2}, \Delta i_{line1} \Delta i_{line2}, \Delta i_{load1}, \Delta i_{load2}, \Delta i_{load3}\right]$.

III. Eigenvalue-Based Analysis For Harmonic Stability

Eigenvalue analysis is a general method to investigate linear system stability, which is able to reveal different frequency components and their damping in the system. To analyze harmonic instability phenomenon, the eigenvalue traces of system state matrix are computed to assess harmonic-frequency characteristic when parameters vary.

A. Harmonic Stability Analysis for Single Inverter

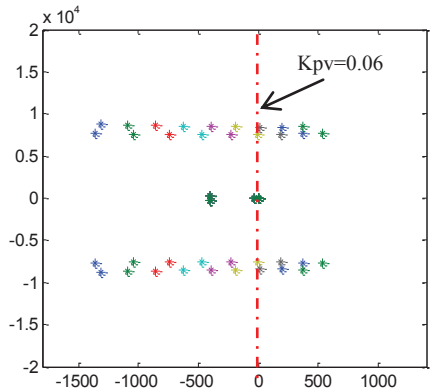

Fig. 5 Eigenvalue trajectory of high frequency modes as a function of the proportional gain of voltage controller (0.01<Kpv<0.09)

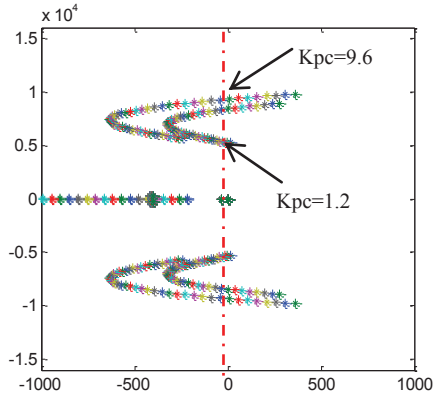

Fig. 6 Eigenvalue trajectory of high frequency modes as a function of the proportional gain of current controller (0.4<Kpc<12)

Fig. 5 depicts the eigenvalue trajectory of single inverter model with loads, where high frequency modes as a function of the proportional gain of voltage controller are shown. It can be seen that two conjugate pairs move towards right-half plane (unstable region) as increase of Kpv from 0.01 to 0.09. The system would be critical stable when Kpv is equal to 0.06.

Fig. 6 shows the eigenvalue trace of high frequency modes as a function of the proportional gain of current controller. It can be seen that the two conjugate pairs move towards right-half plane as decrease of Kpc from 6 to 0.4. Also, the two conjugate pairs move towards right-half plane as increase of Kpc from 6 to 12. The analysis results show that harmonic-frequency instability will happen if the proportional parameter is lower than 1.2 or higher than 9.6.

B. Harmonic Stability Analysis for Paralleled Inverter

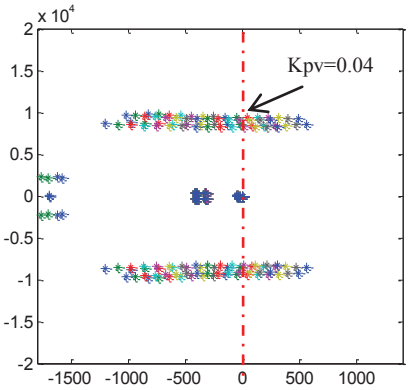

Fig. 7 Eigenvalue trajectory of high frequency modes as a function of the proportional gain of voltage controller (0<Kpv<0.07)

Fig. 7 shows that the eigenvalue traces of small signal model (22) as increase of voltage controller proportional gain. It can be seen that four complex-conjugate pairs dominate harmonic frequency eigenvalues. These eigenvalues are highly sensitive to the proportional gain of voltage controller, where the modes represent dynamics of harmonic frequency range. Eigenvalues analysis shows that the modes move towards right-half plane (unstable region) as Kpv increases.

Fig. 8 shows eigenvalue trace of high frequency modes when the proportional gain of current controller is range from 2 to 12, where the high frequency modes move toward right-half plane as Kpc increases. The system would be instability eventually if Kpc is larger than 10.

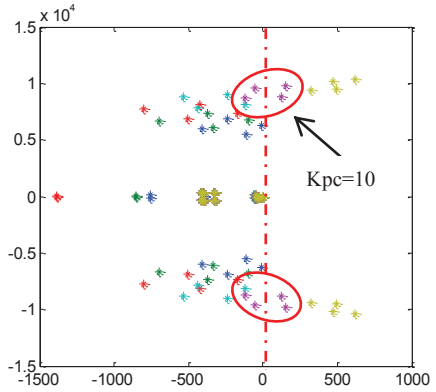

Fig. 8 Eigenvalue trajectory of high frequency modes as a function of the proportional gain of current controller (2<Kpc<12)

IV. Simulation Verification

To validate the proposed eigenvalue-based harmonic stability method, the simulations are performed in MATLAB/SIMULINK. The test system parameters are given in Table I.

Table I Test System Parameters

Parameters	Value	Parameters	Value
L_{f1}/L_{f2}	1.5mH/1.5mH	L_{Line1}/R_{Line1}	2mH/0.2 Ω
C_{f1}/C_{f2}	25μF/25μF	L_{Line2}/R_{Line2}	2mH/0.2 Ω
L_{c1}/L_{c2}	1.8mH/1.8mH	m_{p1}/m_{p2}	2.5e-5/1e-4
T_s	100us	n_{q1}/n_{q2}	1e-3/1e-3
L_{Load1}/R_{Load1}	155mH/64.5 Ω	L_{Load2}/R_{Load2}	156mH/64 Ω
L_{Load3}/R_{Load3}	245mH/80 Ω		

A. Simulation Verification for Single Inverter

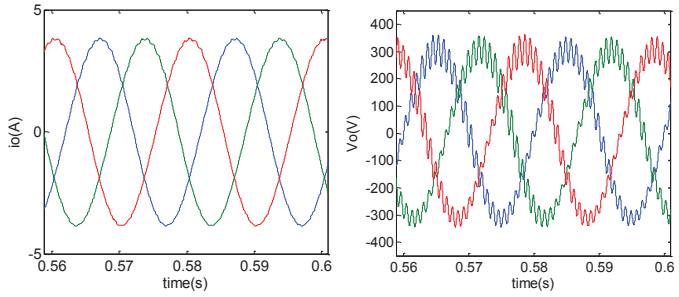

Fig. 9 Simulation results in unstable case. (a) Simulated output current. (b) Simulated output voltage when the proportional gain of voltage controller (Kpv) is 0.074.

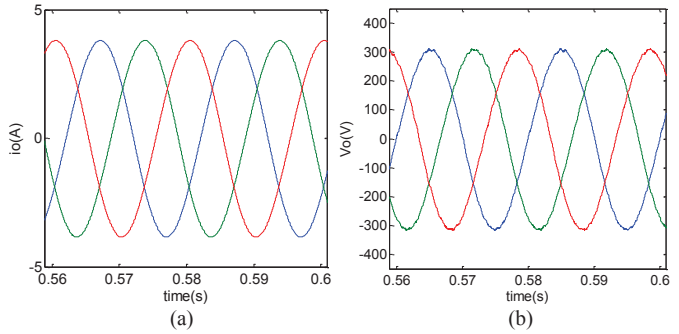

Fig. 10 Simulation results in stable case. (a) Simulated output current. (b) Simulation output voltage after decreasing proportional gain of voltage controller (Kpv=0.05)

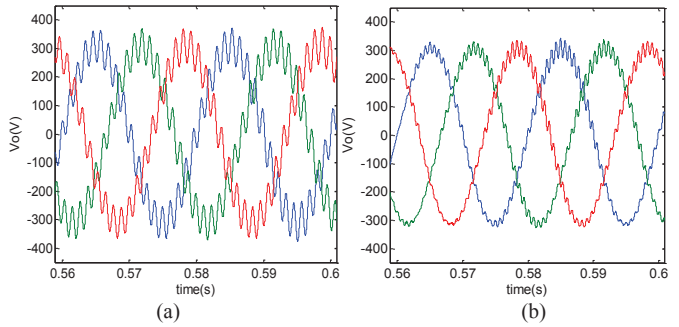

Fig. 11 Simulation results in unstable case. (a) Simulated output voltage (Kpc=0.97). (b) Simulated output voltage (Kpc=12).

Fig. 9 shows that the simulated results for single inverter in unstable case when the proportional gain of voltage controller (Kpv) increase. It can be seen that output voltage will be unstable once the proportional gain is beyond 0.06. In contrast, the output current and output voltage would be stable after reducing the proportional gain of voltage controller (Kpv=0.05) as shown in Fig. 10. The analysis results obtained from Fig. 5 agree with the simulation results.

Fig. 11 depicts that the simulation results for single inverter in unstable case when the proportional gain of voltage controller (Kpc) is 0.97 or 12. It can be seen that the output voltage would be unstable if the proportional parameter is in the unstable region as shown in Fig. 6. As depicted in Fig. 12, the output voltage would be stable when the proportional gain range from 1.2 to 9.6. The simulation results almost agree with the analysis results depicted in Fig.5.

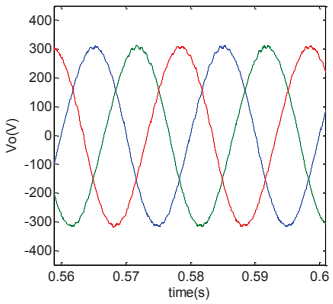

Fig. 12 Simulated output voltage in stable case (Kpc=9)

B. Simulation Verification for Paralleled Inverter

Fig. 13 shows that the simulated results for paralleled inverters in unstable case when the proportional gains (Kpv) of voltage controller vary. The output current of DG units and network voltages are depicted in Fig. 13(a)-(b) and Fig. 13(c)-(d), respectively. It can be seen that harmonic-frequency oscillation happens when the proportional gains (Kpv) of voltage controller are set as 0.053.

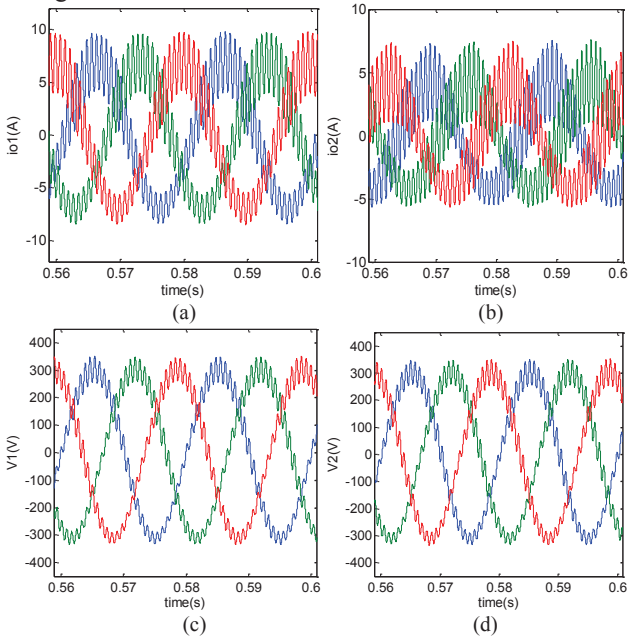

Fig. 13 Simulated results in unstable case when proportional gains of voltage controller (Kpv) is beyond 0.05. (a) DG1 output current. (b) DG2 output current. (c) Bus1 voltage. (d) Bus2 voltage.

Fig. 14 depicts that the simulated results in unstable case when the proportional gains (Kpc) of current controller. The output current of DG units and network voltages are depicted in Fig. 14(a)-(b) and Fig. 14(c)-(d), respectively. It can be seen that harmonic-frequency oscillation still happens when the proportional gains (Kpc) of current controller are set as 12. On the contrary, the output current of DG units and network

voltages are stablized shown in Fig. 15(a)-(b) and Fig. 15(c)-(d) after decreasing the proportional gains of controllers (Kpv=0.035, Kpc=9). The simulation results, together with analysis results shown in Fig. 7 and Fig. 8, indicate that harmonic oscillation happens as the proportional gains of voltage loop and current loop vary.

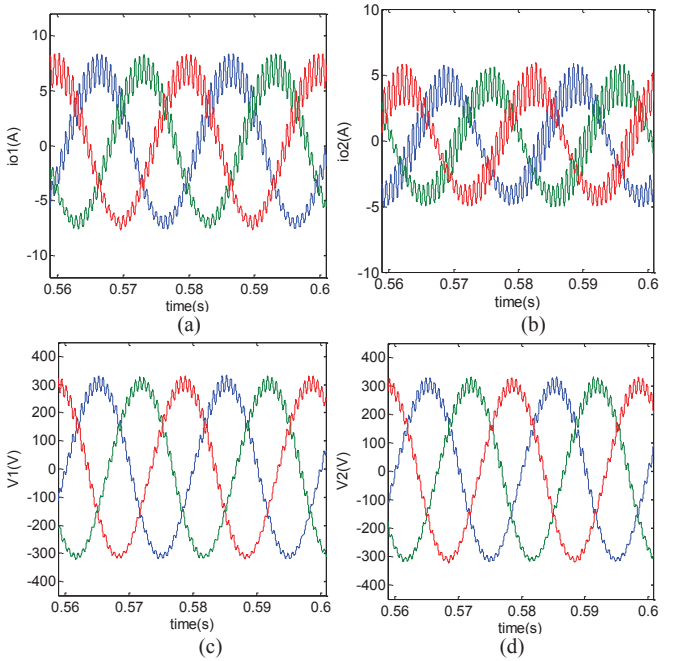

Fig. 14 Simulated results in unstable case when the proportional gain of current controller (Kpc) is in unstable region. (a) DG1 output current. (b) DG2 output current. (c) Bus1 voltage. (d) Bus2 voltage.

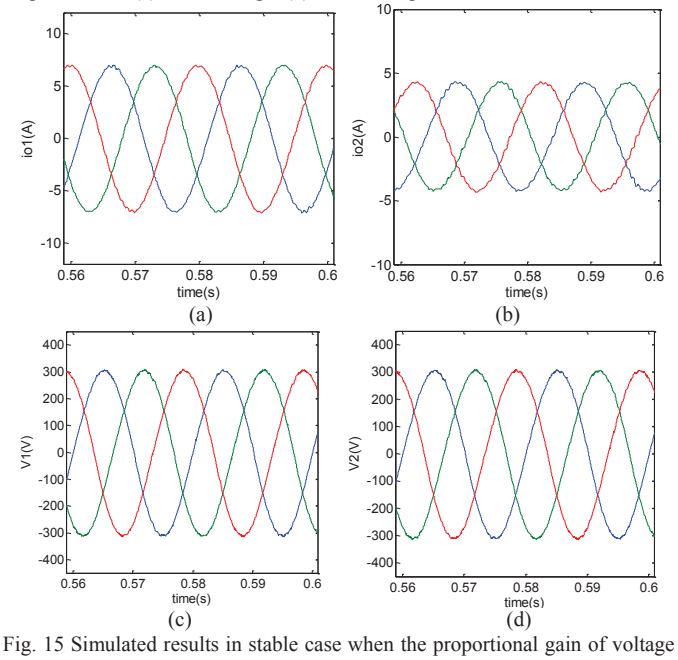

Fig. 15 Simulated results in stable case when the proportional gain of voltage controller (Kpv) is in stable region. (a) DG1 output current. (b) DG2 output current. (c) Bus1 voltage. (d) Bus2 voltage.

CONCLUSIONS

This paper addresses a modeling and analysis method for harmonic stability in inverter-interfaced power systems. An eigenvalue-based analysis method is proposed to assess harmonic instability. First, the small signal model of DG unit including current controller, voltage controller, power controller and inverter delay is built. And the overall small signal model combining DG units, network and loads is developed. Finally, an eigenvalue-based approach is proposed to assess harmonic stability, where the influence of controller parameters on harmonic stability can be assessed through eigenvalue trace diagram. The analytical results show that the proportional gains of inner current controller and voltage controller have an essential effect on harmonic instability in inverter-interfaced power systems. Simulation results are given for validating the proposed harmonic stability analysis method.

ACKNOWLEDGMENT

The authors would like to thank the Danish Council for Strategic Research for providing the financial support project ‘‘Development of a Secure, Economic and Environmentally-friendly Modern Power System’’ (DSF 09-067255)

REFERENCE

[1] R. H. Lasseter, ‘‘Smart distribution: Coupled microgrids,’’ *Proc. IEEE,* vol. 99, no. 6, pp. 1074-1082, Jun. 2011.

[2] Y. Wang, Y. Tian, X. Wang, Z. Chen, and Y. Tan, “Kalman-filter-based state estimation for system information exchange in a multi-bus islanded microgrid,” in *Proc. 7th IET int. Conf. Power Electron, Mach, Drives*, Apr. 8-11, 2014, pp. 1-6.

[3] P. Chen, P. Siano, B. Bak-Jensen, and Z. Chen, ‘‘Stochastic optimization of wind turbine power factor using stochastic model of wind power,’’ IEEE Trans. on Sustainable Energy, vol. 1, no. 1, Apr, 2010.

[4] M. Liserre, R. Teodorescu, and F. Blaabjerg, ‘‘Stability of photovoltaic and wind turbine grid-connected inverters for a large set of grid impedance values,’’ IEEE Trans. on Power electron., vol. 21, no. 1, Jan, 2006.

[5] Y. Wang, Z. Chen, X. Wang, Y. Tian, Y. Tan, and C. Yang, “An Estimator-Based Distributed Voltage-Predictive Control Strategy for AC Islanded Microgrids,” IEEE Trans. on Power Electron, vol. 30, no. 7, Jul, 2015.

[6] X. Wang, F. Blaabjerg, and W. Wu, “Modeling and Analysis of Harmonic Stability in an AC Power-Electronics-Based Power System,” IEEE Trans. on Power Electron, vol. 29, no. 7, Jul, 2015.

[7] N. Pogaku, M. Prodanovic, and T. C. Green, “Modeling, analysis and testing of autonomous operation of an inverter-based microgrid,” IEEE Trans. Power Electron., vol.22, pp. 613-625, Mar, 2007.

[8] N. Bottrell, M. Prodanovic, and T. C. Green, “Dynamic Stability of a Microgrid with An Active Load,” IEEE Trans. Power Electronics, vol.28, no.11, pp. 5107-5119, Nov, 2013.

[9] L. Harnefors, M. Bongiorno, and S. Lundberg, “Input-admittance calculation and shaping for controlled voltage-source converters,” IEEE Trans. Ind. Electron., vol. 54, no. 6, pp. 3323-3334, Dec, 2007.

[10] X. Wang, F. Blaabjerg, M. Liserre, Z. Chen, J. He, and Y. Li, “An active damper for stabilizing power-electronics-based AC systems,” IEEE Trans. Power Electron., vol.29, no.7, pp. 3318-3329, Jul, 2014.

[11] J. Sun, “Impedance-based stability criterion for grid-connected inverters,” IEEE Trans. Power Electron., vol. 26, no. 11, pp. 3075-3078, Nov. 2009.

[12] M. Belkhayat, “ Stability criteria for as power systems with regulated loads,” Ph.D. dissertation, School Electr. Comput. Eng., Purdue Univ., Dec. 1997.

[13] S. Buso, and P. Mattavelli, Digital Control in Power Electronics. CA, USA: Morgen & Claypool Publishers, 2006